HHS Public Access

Author manuscript

Biomaterials. Author manuscript; available in PMC 2016 October 01.

Published in final edited form as:

Biomaterials. 2015 October ; 67: 1–10. doi:10.1016/j.biomaterials.2015.07.028.

Near-infrared fluorescence heptamethine carbocyanine dyes mediate imaging and targeted drug delivery for human brain tumor

Jason Boyang Wu[a,1], **Changhong Shi**[a,b,1], **Gina Chia-Yi Chu**[a], **Qijin Xu**[c], **Yi Zhang**[d], **Qinlong Li**[a], **John S. Yu**[c], **Haiyen E. Zhau**[a], and **Leland W.K. Chung**[a,*]

[a]Uro-Oncology Research Program, Department of Medicine, Cedars-Sinai Medical Center, Los Angeles, CA 90048, USA

[b]Laboratory Animal Center, the Fourth Military Medical University, Xi'an, Shaanxi 710032, China

[c]Department of Neurosurgery, Cedars-Sinai Medical Center, Los Angeles, CA 90048, USA

[d]Biomedical Imaging Research Institute, Cedars-Sinai Medical Center, Los Angeles, CA 90048, USA

Abstract

Brain tumors and brain metastases are among the deadliest malignancies of all human cancers, largely due to the cellular blood-brain and blood-tumor barriers that limit the delivery of imaging and therapeutic agents from the systemic circulation to tumors. Thus, improved strategies for brain tumor visualization and targeted treatment are critically needed. Here we identified and synthesized a group of near-infrared fluorescence (NIRF) heptamethine carbocyanine dyes and derivative NIRF dye-drug conjugates for effective imaging and therapeutic targeting of brain tumors of either primary or metastatic origin in mice, which is mechanistically mediated by tumor hypoxia and organic aniontransporting polypeptide genes. We also demonstrate that these dyes, when conjugated to chemotherapeutic agents such as gemcitabine, significantly restricted the growth of both intracranial glioma xenografts and prostate tumor brain metastases and prolonged survival in mice. These results show promise in the application of NIRF dyes as novel theranostic agents for the detection and treatment of brain tumors.

Keywords

blood brain barrier; brain tumor; drug delivery; heptamethine carbocyanine; hypoxia; near-infrared fluorescence dye

*Corresponding author. Uro-Oncology Research Program, Cedars-Sinai Medical Center, 8750 Beverly Blvd., Atrium 103, Los Angeles, CA 90048, USA. Tel.: +1 3104237622. Leland.Chung@cshs.org (L.W.K. Chung).

[1]These authors contributed equally to this work.

Supplementary Data includes 5 supplementary figures and 1 supplementary table.

1. Introduction

Brain tumors and tumor brain metastases are extremely deadly diseases with poor prognosis and short patient survival. Due to high resistance to chemotherapy and radiotherapy, early surgical intervention after tumor detection by imaging is the standard first-line treatment for most types of brain tumors [1, 2]. The effectiveness of current diagnostics, including computed tomography (CT), magnetic resonance imaging (MRI) and ^{18}F-fluorodeoxyglucose positron emission tomography (FDG-PET) [3, 4], is limited by insufficient specificity and sensitivity, due in part to the background tissue autofluorescence, tissue metabolism, and limited resolution and depth of signal penetration [5, 6]. These limitations may result in significant errors when patients are subjected to imaging for tumor diagnosis, prognosis, and follow-up of therapeutic responses and recurrence. Alternative diagnostic approaches using multimodality opticaland nuclear-imaging-based techniques for the detection of brain tumors and tumor metastatic deposits in the brain are needed.

One central challenge of brain tumor detection and therapy is to deliver diagnostic and therapeutic agents effectively to the tumor core and migratory cells in the infiltration zone [7]. The blood-brain barrier (BBB) and the blood-tumor barrier (BTB) between brain tumor cells and microvessels are major obstacles to the delivery of most agents to tumor tissues from the systemic circulation [7, 8]. Thus, chemotherapy has been of limited benefit for brain tumor patients, due in large part to the poor penetration of drugs through these barriers and the undesired side effects caused by non-selective drug accumulation in healthy tissues [9, 10]. To overcome these barriers, a number of noninvasive targeted approaches, such as peptide-based, nanoparticle-coated delivery platforms [11, 12], have been recently developed as a potential way to deliver targeted agents to brain tumors.

Near-infrared fluorescence (NIRF) imaging agents have great potential for noninvasive tumor imaging [13]. NIRF agents can potentially increase the sensitivity and specificity of cancer diagnosis because NIRF agents have low background autofluorescence, tissue absorbance and scatter at NIR wavelengths (700–1,000 nm) [14]. These agents can also undergo a number of chemical modifications including conjugation with effective therapeutic drugs to target cancer cells at different progressive stages [13, 14]. We previously identified and synthesized a unique group of NIRF heptamethine carbocyanines as dual imaging and targeting agents and demonstrated two prototypic heptamethine carbocyanine dyes including IR-783 and MHI-148. These NIRF and derivative agents show preferential uptake in tumor cells but not normal cells as demonstrated in a variety of cancer cell lines, tumor xenografts, spontaneous mouse tumors in transgenic animals and human tumor samples [15–18], mediated by tumor hypoxia and activated hypoxia-inducible factor 1α (HIF1α)/organic anion-transporting polypeptides (OATPs) signaling axis [17, 19]. However, whether these dyes possess the potential to penetrate the BBB/BTB and target brain tumors had not been evaluated. In this study, using a number of *in vitro* and *in vivo* brain tumor models, we investigated the mechanisms and targeting potential of this group of NIRF agents for primary and metastatic brain tumors. We also evaluated the ability of these dyes as carriers to deliver dye-drug conjugates to brain tumors and the therapeutic efficacy of these conjugates in mouse models.

2. Materials and methods

2.1. Cell culture and reagents

Human glioblastoma cell lines U87, U251 and T98G, and normal human embryonic kidney cell line HEK293 were purchased from American Type Culture Collection (ATCC, Manassas, VA). Human prostate adenocarcinoma cell line CW22Rv1 was kindly provided by Dr. Michael Freeman (Cedars-Sinai Medical Center, Los Angeles). These cells were cultured in Dulbecco's modified Eagle's medium (DMEM; Life Technologies, Grand Island, NY) or RPMI 1640 medium (Life Technologies) supplemented with 10% FBS (Biowest, Kansas City, MO) and 1% penicillin/streptomycin (Life Technologies). Human brain cancer stem-like cells (CSCs) isolated from pituitary adenoma patients were prepared as described previously [20] and cultured in a DMEM/F12 (1:1) medium (Life Technologies) containing B27 (1×) supplement (Life Technologies), 1% penicillin/streptomycin, fungizone (250 ng/ml; Life Technologies), EGF (20 ng/ml; Peprotech, Rocky Hills, NJ) and bFGF (20 ng/ml; Peprotech). For hypoxia treatment, cells were grown in a hypoxic chamber (1% O_2, 5% CO_2). Lentiviral particles expressing both luciferase and GFP were purchased from GenTarget (San Diego, CA). Bromosulfophthalein (BSP), cobalt chloride ($CoCl_2$) and dimethyloxalylglycine (DMOG) were purchased from Sigma-Aldrich (St. Louis, MO). D-Luciferin sodium salt was purchased from Gold Biotechnology (St. Louis, MO). The heptamethine carbocyanine dye IR-783 was prepared and purified as described previously [15]. Gemcitabine was purchased from Ark Pharm, Inc. (Libertyville, IL). All other chemicals used in IR-783- gemcitabine (NIRG) synthesis were purchased from Sigma Aldrich. NIRG was synthesized in house with detailed synthesis procedures described below.

2.2. IR-783-gemcitabine (NIRG) synthesis

The preparation of the compound 4-(2-((E)-2-((E)-2-chloro-3-(phenylamino)methylene)-cyclohex-1-en-1-yl)vinyl)-3, 3-dimethyl-3H-indol-1-ium-1-yl)butane-1-sulfonate 3—To the mixture of **1a** (2 g, 6.78 mmol) and crude 2 (3 g, 8.36 mmol) in EtOH (25ml) was added CH_3COONa (0.56 g, 6.78 mmol), the resulted mixture was heated to reflux for 3 h. The reaction mixture was concentrated and the residue was recrystallized from methanol/ether to afford desired product **3** (2 g, yield 56%). HRMS (ESI-TOF), m/z 525.1979 $(M+H)^+$ ($C_{29}H_{34}ClN_2O_3S$ requires 525.1979).

The preparation of the compound cyanine dye 4—To the mixture of **1b** (0.5 g, 1.4 mmol) and crude **3** (1 g, 1.9 mmol) in EtOH (8 ml) was added CH_3COONa (128 mg, 1.5 mmol), the resulted reaction was heated to reflux for 3 h. The reaction mixture was concentrated and the residue was purified with C18-RP silica chromatography elution with methanol-water to afford desired product **4** (0.8 g, yield 73%). ^1H NMR (DMSO-d6, 400 MHz) HRMS (ESI-TOF), 705.3122 $(M+H)^+$ ($C_{40}H_{50}ClN_2O_5S$ requires 705.3129).

The preparation of the compound dye-gemcitabine conjugate 5—The mixture of **4** (761 mg, 1.1 mmol) 1-ethyl-3-(3-dimethyllaminopropyl) carbodiiehydrochlide (310 mg, 1.6 mmol) and 1-hydroxy-7-azabenzotriazole (175 mg, 1.3 mmol) were dissolved in 5.0 mL DMF solution. The mixture was stirred for 15 min, then gemcitabine (340 mg, 1.3 mmol)

was added and stirred for additional 15 hours. Ethyl ether (50 ml) was added. The precipitate collected and purified by C18-RP silica chromatography was eluted with methanol-water to afford desired product 509 mg (41%). HRMS (ESI-TOF), m/z 948.3578 $(M-H)^-$ ($C_{49}H_{57}ClF_2N_5O_8S$ requires 948.3585).

ESI-TOF-MS analysis was performed on compounds at the UCLA Mass Spectrometry Laboratory using a Waters LCT Premier Mass Spectrometer. Protein nuclear magnetic resonance (^{1}H NMR) spectra were recorded on a Bruker AV400 FT NMR Spectrometer (400 MHz)

2.3. Tumor xenograft studies

All animal studies received prior approval from the IACUC of Cedars-Sinai Medical Center (CSMC) and were conducted in compliance with its recommendations. Male 4- to 6-week-old athymic nude mice and SCID mice were purchased from Taconic (Oxnard, CA), housed in the animal research facility at CSMC, and fed a normal chow diet. For subcutaneous xenograft studies, 1, 3 or 9×10^6 of luc-labeled U87 in 50% Matrigel (BD Biosciences, San Jose, CA) were injected subcutaneously into nude mice. Each mouse was injected on the right flank only. Tumor size was measured by caliper. For intracranial xenograft studies, SCID or nude mice were anesthetized by intraperitoneal injection of ketamine and xylazine, and stereotactically implanted with U87 or pituitary adenoma CSC cells (10,000 cells per mouse), respectively, in the right forebrains. At the end of the studies, tumor-bearing whole mouse brains were excised and fixed in 10% formaldehyde and embedded in paraffin for subsequent histological analysis. For intracardiac xenograft studies, 1×10^6 luc-tagged CW22Rv1 cells were injected into the left cardiac ventricle of anesthetized SCID mice as described previously [21]. Development of brain metastasis was monitored by BLI and MRI.

2.4. Bioluminescence Imaging

Bioluminescence imaging of luciferase-tagged U87 or CW22Rv1 tumor xenografts either *in vivo* or *ex vivo* after mice received D-luciferin (3 mg/mouse via intraperitoneal delivery) was performed on a Xenogen IVIS Spectrum Imaging System (PerkinElmer, Waltham, MA). Analysis was performed with Living Image software (PerkinElmer) by measurement of photon flux in the tumor region of interest in mice. Data was normalized to the background signal.

2.5. Magnetic Resonance Imaging

MRI experiments were performed on a 9.4T (94/20) Bruker BioSpec MRI scanner (Bruker, Billerica, MA) using 4 channel ^{1}H mouse brain receiver coil (Bruker). The tumor-bearing mouse brain was excised and placed in 10% formaldehyde for at least 24 hours then suspended in Fomblin® YLVAC (Sigma-Aldrich) for imaging. T1 weighted 0.5 mm axial slices, encompassing the whole brain (50 slices), were acquired with a fast spin echo sequence to delineate anatomic details with an in-plane resolution of 92 μm (field of view, 18 mm × 12 mm; TE/TR, 8 ms/900 ms, 196 × 128 matrix, 6 averages). MRI data were processed and analyzed using ParaVision software (Bruker).

2.6. Analysis of brain tumor imaging and targeting by NIRF dye and NIRG in cultured brain tumor cells and xenografts

For cultured brain and prostate tumor cells, after exposure to different treatments when necessary, cells were incubated with IR-783 at a concentration of 20 μM at 37°C for 30 min and washed twice with PBS to remove excess dye. Cells were either fixed in 10% formaldehyde when cultured alone or incubated in PBS when present in co-culture, and subjected to analysis of NIRF dye uptake by NIRF microscopy (Olympus 1×71; Olympus, Melville, NY) using a 75 W Xenon lamp and an indo-cyanine green filter cube (excitation/emission: 750–800/820–860 nm) as described previously [15]. Cellular NIRF intensity was quantitated by ImageJ software (NIH). For tumor xenograft models, mice bearing xenograft tumors were injected intraperitoneally with IR-783 or NIRG at a dose of 50 nmol/mouse assuming the average body weight of mice is 20 grams. Whole-body or organ-specific optical imaging was taken at 1 hour or/and 24 hour using an IVIS Lumina XR Imaging System (PerkinElmer, Waltham, MA) equipped with fluorescent filter sets (excitation/emission, 783/840 nm), with automatic subtraction of background fluorescence from the total dye uptake in tumors during the image acquisition, as described previously [15, 22].

2.7. Biochemical analyses of brain tumor cells and tumor xenografts

Total RNA from cultured cells and formalin-fixed, paraffin-embedded tissue sections was isolated using the RNeasy Mini Kit and the RNeasy FFPE Kit (Qiagen), respectively; and reverse-transcribed to cDNA by M-MLV reverse transcriptase (Promega) following the manufacture's instructions. qPCR was conducted using SYBR Green PCR Master Mix and run with Applied Biosystems 7500 Fast Real-Time PCR System (Applied Biosystems). PCR conditions include an initial denaturation step of 3 min at 95°C, followed by 40 cycles of PCR consisting of 30 s at 95°C, 30 s at 60°C, and 30 s at 72°C. The PCR data were analyzed by $2^{-\Delta\Delta CT}$ methods [23]. Details on primers used for qPCR are provided in the Supplementary Table 1.

2.8. Microarray data sets

Two brain cancer DNA microarray data sets, Bredel Brain 2 [24] and Sun Brain [25], were downloaded directly from the Oncomine database by licensed access. Microarray data of the Bredel Brain 2 (GSE2223) and Sun Brain (GSE4290) data set are also publicly available in Gene Expression Omnibus.

2.9. Cell proliferation assays

U87 cells were seeded at 3,000/well in a 96-well plate and treated with either gemcitabine (200 nM) or IR-783-gemcitabine (200 nM) for 4 consecutive days. PBS was used as a vehicle. Cells were fixed and stained with crystal violet, and the OD value at the wavelength of 595 nm was read by a microplate reader on a daily basis.

2.10. Tumor xenograft therapeutic studies

For determining the therapeutic effect of NIRG on brain tumor or metastasis, mice bearing either intracranial U87 tumors or CW22Rv1 prostate tumor brain metastases as confirmed by BLI were randomly assigned to 2 groups. For U87 tumor model, 2 weeks after tumor cell

inoculation, mice were injected intraperitoneally with either saline or NIRG (10 mg/kg) twice a week for 4–5 weeks. For CW22Rv1 prostate tumor brain metastatic model, after confirming the presence of tumor metastases in mouse brains, mice were injected intraperitoneally with either saline or NIRG (10 mg/kg) twice a week for 5 weeks. Tumor growth and development of brain metastasis were monitored by BLI.

2.11. Statistical analysis

Data were presented as the mean ± SEM as indicated in the figure legends. Comparisons between Kaplan-Meier curves were performed using the long-rank test. All other comparisons were analyzed by unpaired 2-tailed Student's *t* test. A *p* value less than 0.05 was considered as statistically significant.

3. Results

3.1. Preferential accumulation of NIRF dye in brain tumor cells

Glioblastoma, the most common and aggressive malignant primary brain tumor arising from astrocytes [2], was chosen as a model to assess the ability of NIRF dye uptake by brain tumor cells and xenografts. To determine whether the NIRF dye specifically targets brain tumor cells but not normal cells, we established an *in vitro* co-culture model in which human glioblastoma U87 cells were engineered dually with green fluorescence protein (GFP) and luciferase (luc) and cultured together with normal human embryonic kidney HEK293 cells in a 2-dimensional culture on a plastic surface. Lentiviral infection-mediated labeling of U87 cells with GFP followed by puromycin selection ensured a 100% integrated rate of GFP in stable U87 cells, which was confirmed by fluorescence microscopy (Fig. S1). To examine the dye uptake, the coculture was incubated with IR-783, a NIRF heptamethine carbocyanine dye we identified previously (chemical structure shown in Fig. 1A), and then subjected to fluorescence microscopy. The NIRF signals were exclusively observed in GFP^+ U87 cells and not in the other GFP^- HEK293 cells (Fig. 1B), suggesting the preferential uptake and retention of IR-783 in brain tumor cells but not normal cells under the same culture conditions. We also examined the dye uptake in this co-culture model in a quantitative manner. A doubling series number of luc-tagged U87 cells were incubated with a fixed number of HEK293 cells, producing different cell number ratios (U87/HEK293 1:8, 1:4, 1:2 and 1:1). These co-cultures were exposed to IR-783 and subjected in parallel to luminescence and NIRF imaging, demonstrating a significant linear correlation (R^2=0.9958) between luminescence and NIRF signal intensities (Figs. 1C and 1D), which reinforces the finding of a preferential dye uptake by brain tumor cells relative to normal cells. These results in aggregate confirm the tumor-specific targeting ability of IR-783 dye in cultured brain tumor cells.

3.2. NIRF dye uptake correlates with brain tumor xenograft growth

To determine whether the preferential uptake of IR-783 by brain tumor cells *in vitro* can be recapitulated *in vivo*, we implanted different numbers (1×10^6, 3×10^6 and 9×10^6) of luc-tagged U87 cells subcutaneously into nude mice to establish tumor xenografts. When tumors formed at different sizes as expected, we demonstrated by whole-body NIRF imaging that IR-783 was specifically taken up by xenograft tumors in mice. This was further supported

by the co-registered bioluminescence (BLI) and NIRF signals in tumors, with a positive correlation (R^2=0.9980) of signal intensity between the two imaging modalities (Fig. 2B). Moreover, a significant correlation (R^2=0.9811) between tumor NIRF signal intensity and tumor volume was established (Fig. 2C). Immediately after *in vivo* imaging, tumors were dissected and analyzed *ex vivo* by both BLI and NIRF imaging simultaneously (Fig. 2D). Similarly, we showed that tumor NIRF signal intensity was well correlated with both tumor BLI intensity (R^2=0.9973) and tumor weight (R^2=0.9830) (Figs. 2E and 2F). In addition, we observed marginal dye uptake by other normal mouse organs, such as the lung, heart, spleen, kidney and liver, consistent with our previous results [15, 22]. Together, these results indicate the ability of IR-783 to target specifically brain tumor in a subcutaneous model and more importantly to quantitatively estimate tumor burden in mice.

3.3. NIRF dye penetrates the BBB/BTB and targets intracranial brain tumor xenografts

A unique feature of brain tumors is the presence of tight barriers, termed BBB and BTB, which protect cancer cells from exposure to most chemical agents in circulation[8]. To assess whether IR-783 can target brain tumors at the primary site, we generated an intracranial brain tumor xenograft by stereotactically implanting U87 cells into the right hemisphere of immunocompromised mice. Once the intracranial tumor xenograft was established, mice were given IR-783 through the intraperitoneal route to allow the delivery of this NIRF dye by systemic circulation. At 1 hour and 24 hours after the dye injection, mice were subjected to NIRF imaging. The results showed that NIRF signals localized exclusively in the brain region in mice in a time-dependent manner (Fig. 3A, left panel), indicating that IR-783 was capable of passing through the BBB/BTB and entering the tumor core space. In contrast, we did not observe the accumulation of IR-783 dye in the sham-operated normal brain that did not harbor tumor by *in vivo* imaging (Fig. 3a, right panel). A signal-to-background ratio (tumor/no tumor) ranging from 2.9 to 5.6 was observed at different time points (Fig. 3B). We also assessed the brain tumortargeting ability of IR-783 dye by *ex vivo* imaging of an alignment of individual mouse organs, demonstrating the presence of NIRF signals only in the brain and not in other selected major organs including the lung, heart, spleen, kidney and liver (Fig. 3C). Quantitative analysis of the organ-specific accumulation of dye intensity showed an average of 81.6-fold higher NIRF intensity in the brain than the average intensity in other organs (Fig. 3D).

To better mimic the clinical situation, we implanted human pituitary adenoma stemlike cells prepared directly from patient samples into the brains of nude mice. As demonstrated by both *in vivo* and *ex vivo* NIRF imaging (Figs. 3E and 3F), IR-783 was taken up specifically by the tumor-bearing brains in mice, which further showed up to 82.6-fold higher NIRF signal intensity in the brain compared to that in other selected organs (Fig. 3G). In line with these data, we conclude that NIRF dye can be taken up by brain tumors after effectively penetrating the BBB/BTB.

3.4. Hypoxia and organic anion-transporting polypeptide (OATP) genes mediate NIRF dye uptake into brain tumor cells

We recently showed that hypoxia mediates the uptake of NIRF dye by cancer cells via activation of HIF1α/OATP signaling in a series of genitourinary cancer models [22]. This

provides insights into brain tumor, where hypoxia is also frequently observed due to inadequate vascular supply or inefficient microcirculation in vascularized tumor regions [26]. OATPs could also mediate the uptake of NIRF dyes including both IR-783 and MHI-148 [22]. OATPs represent a superfamily of solute carrier transporter, including 11 known human OATPs classified into 6 families and subfamilies on the basis of their amino acid sequence homologies [27]. Aberrant expression of OATPs has been reported in a spectrum of cancer types, including brain cancer [28, 29]. OATPs facilitate the transport of a number of substances into cells, including organic acids, drugs and hormones, in a highly substrate- and pathophysiologic- including cancer-dependent manner [27]. Notably, select OATPs including OATP1A2 and OATP2B1 are highly expressed in physiological barriers such as the BBB [30], and a significantly lower bloodto- brain transport of several agents was observed in *Oatp1a4* (corresponding to *OATP1A2* in humans) knockout mice compared to wild-type mice [31]. These studies in aggregate suggest a potential role of these OATPs in depositing contrast agents and drugs into brain tumors.

Given the common features, including hypoxia and aberrant expression of OATPs, shared by brain tumors and other types of tumors, we speculated whether brain tumor cells use similar mechanisms to take up and retain NIRF dyes. To test this, three human glioblastoma cell lines, U87, U251 and T98G, were exposed to IR-783 under hypoxic conditions (1% O_2). As shown in Figs. 4A, 4B and S2, there were significant increases in dye uptake varying from 41% to 149% after hypoxic stimuli in all three cell lines. Moreover, cells pre-treated with bromosulfophthalein (BSP), a potent competitive inhibitor of OATPs, reduced dye uptake by up to 64% in all cell lines (Figs. 4A, 4B and S2). These data collectively suggest that hypoxia and OATPs mediate the uptake of NIRF dye in brain tumor cells.

Next, we examined the expression levels of select brain-related OATPs in U87 intracranial tumor xenograft samples. As shown in Fig. S3A, higher mRNA expression of 3 *OATP*s, including *OATP1A2*, *OATP1C1*, and *OATP2B1*, was found in U87 tumor than nearby normal mouse brain tissue, which is supported by the observations of increased *OATP2B1* expression in glioblastoma samples compared with normal brain tissues in 2 brain cancer clinical data sets (Fig. S3B, Bredel Brain 2 and Sun Brain). To further determine if the hypoxia upregulation of OATP expression as we reported previously could be recapitulated in the scenario of brain tumor [19], we treated U87 cells with cobalt chloride or DMOG, two hypoxia-mimetic agents stabilizing the expression of HIF1α, a master regulator of hypoxia signaling [19, 32, 33]. Induction of hypoxia, evidenced by increased expression of vascular endothelial growth factor A (VEGFA) and glucose transporter 1 (Glut1), two HIF1α-target genes, activated the expression of select brain-expressing *OATP*s, including *OATP1A2*, *OATP1C1*, and *OATP2B1*, in U87 cells under both treatments (Fig. S3C). Furthermore, we demonstrated a significant correlation between *HIF1α* and *OATP2B1* mRNA expression in the Sun Brain data set (Fig. S3D, p=0003 and p<0.0001 for Pearson and Spearman correlation, respectively). These results reinforce OATPs' function to facilitate the delivery of NIRF dyes across the BBB/BTB via an increased OATPs gradient across brain tumor cell membranes for dye uptake by brain tumors.

3.5. NIRF dye as a drug delivery carrier for therapeutically targeting brain tumors and brain metastases

Given the ability of IR-783 to target brain tumors specifically in different intracranial models (Fig. 3), we next investigated the potential of IR-783 as a drug delivery carrier covalently linked to a drug payload to serve as a theranostic agent for both imaging and antitumor capabilities. To develop IR-783 as a platform for drug delivery, we synthesized and characterized a modified compound that conjugates gemcitabine with a derivative of IR-783 backbone with one sulfonate moiety converted to carboxylate (IR-783-gemcitabine, abbreviated as NIRG) (Figs. 5A and S4), and tested its activity against the growth of brain tumor xenografts and prostate tumor metastasized to mouse brain. This conjugation with appropriate modification of one side chain of the heptamethine carbocyanine dye dose not change the electronic properties of the aromatic backbones in order to maintain the fluorescence and tumor-specific targeting properties. On the other hand, conjugation of gemcitabine at the 4-(N)-amino group in the pyrimidine ring via amide bond has emerged as one of the most versatile methods for producing gemcitabine prodrugs without compromising drug activity [34, 35]. Gemcitabine is a deoxycytidine analog that has shown a wide range of antitumor activity against the proliferation of different solid tumors, such as lung cancer, pancreatic cancer and breast cancer [36–38], by directly interfering with DNA replication to arrest tumor growth [39, 40]. Gemcitabine at non-cytotoxic concentrations enables brain tumor radiosensitization [41]. However, it shows only modest potency to penetrate the BBB, resulting in limited therapeutic benefits for intracranial tumors [42]. We first characterized the fluorescence-emitting and cellkilling functions of NIRG. In parallel to IR-783, U87 cells retaining NIRG demonstrated strong NIRF signals (Fig. S5A, left panel), indicating the intact property of the carbocyanine dye to emit fluorescent photons for imaging. NIRG was also observed to inhibit the proliferation of U87 cells when compared to that of the vehicle-treated group (Fig. S5B), indicating its cytotoxic effect through the functional group of drug payload, gemcitabine. We next determined the uptake of NIRG by intracranial U87 tumors in mice. As shown by whole-body NIRF imaging (Fig. 5B), the conjugate was able to penetrate the BBB/BTB and was taken up specifically by tumor-bearing brains in mice with a timedependent increase in signal intensity (1 hr vs. 24 hr), with signal-to-background ratios (tumor/no tumor) ranging from 3.5 to 4.2 at different time points (Fig. 5C). *Ex vivo* NIRF imaging confirmed significantly enhanced retention of NIRG in mouse brain relative to other organs with an increase up to 7.9-fold in signal intensity (Figs. 5D and 5E). Importantly, NIRG treatment significantly reduced the growth of intracranial U87 tumors in mice without affecting body weights of mice as compared to the control group (Figs. S5C and S5D), which suggests that NIRG has utility as an effective dual imaging and therapeutic agent for brain tumor.

In addition to the primary brain tumor, brain metastases can be developed by prostate, breast and lung cancers. Though brain is not as frequent a metastatic site as other distant organs, such as the skeleton, lethality from brain metastases occur frequently due in part to the lack of effective treatment strategies [43, 44]. To test the potential of NIRG for targeting metastatic brain lesions, we first generated an intracardiac tumor xenograft model in immunodeficient mice by injecting a luc-tagged CW22Rv1 human prostate cancer cell line that is known to retain NIRG *in vitro* (Fig. S5A, right panel), as a model for the study of

NIRG as a theranostic agent for prostate cancer brain metastases [45]. Mice that developed brain metastases after inoculation was confirmed by BLI received NIRG at 10 mg/kg intraperitoneally and were then subjected to dual modalities of BLI and NIRF imaging. Both *in vivo* and *ex vivo* imaging analyses showed co-registered BLI and NIRF signals accumulating specifically in the brain but not in other organs in mice (Figs. 6A and 6B), with a brain-to-kidney signal ratio of 102.5 and 30.6 for BLI and NIRF imaging, respectively (Fig. 6C). The brain lesions were confirmed by MRI (Fig. 6D) and H&E stain (Fig. 6E). Our results further demonstrated significantly improved survival in mice receiving NIRG for 5 consecutive weeks as compared to saline-treated control mice (Fig. S5E). These data in aggregate establish the potential use of NIRF dyes for guiding the targeted delivery of therapeutic drugs to brain tumors and brain metastases for effective therapeutic intervention.

4. Discussion

Brain tumors are one of the most deadly tumors in both adults and children [1, 2]. Glioblastoma, the most common malignant primary brain tumor in adults, is the second cause of cancer death in adults less than 35 years of age and shows a survival rate of less than 10% after diagnosis [46, 47]. Despite surgical and medical advances achieved in recent years, the prognosis for brain tumor patients still remains poor. These dismal facts underscore the importance of pursuing alternative solutions for improved brain tumor diagnosis and therapy. In addition, since there are currently a plethora of different imaging techniques available, multimodality approaches are attractive by offering companion diagnostics while subjecting the patients to imaging-guided therapy. This was illustrated by recent studies using triple-modality MRI-photoacoustic imaging-Raman imaging nanoparticles for more accurate delineation of brain tumor margins for surgical resection compared to a single imaging modality [48].

In this study, we demonstrated that a group of NIRF heptamethine carbocyanine dyes, IR-783 dye and its conjugate, NIRG, provided highly effective tools for noninvasive brain tumor imaging and targeting. In contrast to conventional dyes in cancer imaging which require chemical conjugation of the imaging probes with appropriate tumor-specific ligands, such as chemical substrates, aptamers, growth factors or antibodies that recognize cell surface receptors in experimental mouse models [49–51], the uptake of NIRF dyes is dependent upon tumor hypoxia and the intrinsic expression of OATPs so that their entry into tumor cells does not require chemical conjugation[19]. These attractive features of NIRF dyes have distinct advantages to allow simple and straightforward detection of brain tumors and brain metastases by imaging agents with smaller sizes compared to other dyes where large molecules resulting from chemical conjugation often compromise their ability to penetrate the BBB/BTB [9]. We showed the preferential uptake of IR-783 by brain tumor cells and intracranial tumor xenografts in mice (Figs. 1 and 3). We also showed a significant correlation between tumor NIRF signal intensity and brain tumor burden in a subcutaneous tumor growth model (Fig. 2), indicating the potential uses of NIRF dye for tumor localization and quantitative imaging, which would greatly complement existing modalities for the imaging-assisted diagnosis and prognosis of brain tumors. Of note, not all cyanine dyes have tumor-targeting properties despite their structural resemblance to each other. Only

heptamethine carbocyanine dyes that have charged side-chain terminal groups and a chlorine atom at the central meso position of the cyclohexyl ring are cancer-specific and able to cross the BBB. In addition, the negative charges owned by IR-783 and its derivative dyes such as MHI-148 by possessing a sulfate or carboxyl group allow these dyes to be efficiently mediated by OATPs for BBB penetration [15, 19].

In addition to primary brain tumors, the highly infiltrating nature of glioblastoma and the presence of migratory cells in the infiltration zone protected by the BBB is a major cause of brain tumor lethality in affected patients [1, 9]. Conventional surgical methods cannot completely remove these invasive tumor cells outside the tumor bulk largely due to the intraoperative difficulties in delineating the brain tumor margins precisely, which inevitably leads to tumor relapse following surgery [1, 48]. Given the high sensitivity and specificity of these NIRF dyes for targeting brain tumor cells at the cellular level (Fig. 1), extending the application of these dyes for assessing brain tumor margins for improved surgical outcomes merits further investigation.

We showed that hypoxia is one of the mechanisms responsible for the preferential uptake of NIRF dye by brain tumor cells (Fig. 4), a result consistent with our previous findings [22]. It is evident that hypoxia generally exists in brain tumors, the obvious direct evidence being the presence of intratumoral necrosis, which in fact underlies the histological diagnosis of glioblastoma [52]. The hypoxia-mediated dye uptake mechanism may allow these NIRF dyes to target a broad range of brain tumor types despite their heterogeneous nature. One challenge to conventional imaging evaluation for brain tumor diagnosis is the occasional inability to distinguish radiation-induced necrosis or treatment-related pseudoprogression from recurrent high-grade tumor [52, 53]. These post-treatment entities that mimic tumor recurrence have been suggested to correlate with treatment-related cellular hypoxia, leading to expression of hypoxia-regulated molecules from tumor and surrounding cells with subsequent increased vascular permeability and increased tumor enhancement [52]. We previously demonstrated a positive correlation between tumor uptake of NIRF dye and the extent of hypoxia using a HIF1α-dependent luciferase reporter in mice [22, 54]. These dyes collectively may be useful for evaluating residual or recurrent live tumors following treatment by measuring the level of tumor hypoxia for improved diagnostic and prognostic accuracy and therapeutic responsiveness.

In addition to hypoxia, we showed that OATPs are another regulatory mechanism mediating NIRF dye uptake by brain tumor cells (Fig. 4). OATPs mediate the transmembrane uptake of amphipathic compounds, including drugs, hormones and other xenobiotics that cannot freely diffuse through cellular membranes, thereby affecting drug disposition and tissue penetration. Recent evidence has implicated altered OATP expressions and variants in many different types of cancers, including OATP1A2 and OATP2B1 in brain cancer [27–29, 55]. Their expression in the luminal membrane of endothelial cells forming the BBB and BTB and the following evidence indicating reduced blood-to-brain transport of several agents in mice without *Oatp1a4*, a form corresponding to *OATP1A2* in humans, suggest the role of these OATPs in facilitating the NIRF dye to penetrate the barriers and enter brain tumors [30, 31]. We have previously demonstrated that tumor cell uptake of these NIRF dyes can be mediated by OATPs, which is further enhanced by tumor hypoxia through the direct

upregulation of OATPs by HIF1α at the transcriptional level, resulting in a concerted effect on increased uptake of NIRF dye by tumor cells. [15, 19, 56, 57]. In the present brain tumor study, we showed a similar dye uptake mechanism mediated by OATPs (Figs. 4 and S2), which could be either responsive to hypoxic effects or independent from tumor hypoxia. In agreement with our previous studies, the expression of several OATPs abundant in the BBB/BTB and brain tumor was elevated in brain tumor cells under hypoxia-mimicking conditions, which is further associated with a significant co-expression correlation between *HIF1α* and *OATP2B1*, a representative *OATP*, in a clinical brain tumor data set (Fig. S3). On the other hand, we showed that pharmacological blockade of OATPs activities by a competitive inhibitor under normoxic conditions was sufficient to inhibit the dye uptake by brain tumor cells (Figs. 4 and S2). Importantly, we demonstrated increased expression of several brain-expressing forms of OATPs in the intracranial U87 tumor relative to nearby normal mouse brain tissue in mice subjected to NIRF imaging, which is consistent with the clinical observation of higher expression of these OATPs in glioblastoma than normal brain tissues (Fig. S3). These results suggest that even without hypoxia the prevailing activation of OATPs in brain tumors is able to facilitate dye delivery across the BBB/BTB and dye uptake in brain tumors *in vivo*.

We demonstrated the preferential uptake of IR-783 by brain tumors in an intracranial xenograft model as early as 1 hour after dye injection (Fig. 3), further with a time-dependent increase in dye uptake at 24 hours, suggesting a tumor-attractive distribution of IR-783 in the body. We have previously reported the whole-body distribution of IR-783 dye at a series of time points starting from 0.5 hour after dye administration in tumor-bearing mice. In addition to specific retention in tumors, IR-783 was shown to accumulate in liver, kidney heart, lung and spleen for up to 6 hours followed by clearance from these normal organs. However, normal organs displayed very low signals likely to be overshadowed by the more intense signals in tumors during imaging [15]. In addition, the observation of a time-dependent increase in dye uptake in tumors also fits the dye uptake model we demonstrated where IR-783 dye was progressively accumulated in brain tumors, mediated by OATP-based active transport, after the dye was rapidly diffused into the bloodstream and distributed in the whole body by circulation since injection. By contrast, normal organs and tissues retained dyes poorly due in large part to the lack of OATP involvement given the low expression of OATPs, thereby producing marginally detectable focal fluorescence signals by imaging. Increased dye uptake in brain tumors along with time supports an OATP-mediated redistribution of dyes from non-target normal organs to brain tumors in the body.

Chemotherapy is indispensable for brain tumor treatment after surgery [10], but its limited benefits are due to the ineffective delivery of therapeutic agents to the tumor tissues as well as undesired side effects elicited by nonspecific biodistribution [9, 10]. In this study, we overcame these problems using NIRF dye as a drug carrier covalently conjugated to chemotherapeutic agents, facilitating the ability of drugs to penetrate the BBB/BTB. Using gemcitabine as an example, we demonstrated the exclusive accumulation of the NIRG conjugate in intracranial human tumors and brain tumor metastases in a human prostate cancer model (Figs. 5 and 6). We showed that NIRG is capable of restricting the growth of intracranial brain tumors and prostate tumor brain metastases and prolonging the survival of

mice (Fig. S5). Because NIRF dye and NIRG can accumulate in tumor tissues and cells for a prolonged period due to their extensive interaction with cellular nucleic acids and proteins [58, 59], these dyes and dye-drug conjugates could be further explored as promising imaging and targeting agents for the imaging and treatment of primary and metastatic brain tumors.

5. Conclusions

In this study, we demonstrated that NIRF dyes and derivative dye-drug conjugates, such as NIRG, are effective and promising new imaging and targeting agents for the detection and treatment of human brain tumors and brain metastases. The uptake and retention of these agents by brain tumors are mediated by tumor hypoxia and OATPs in the BBB/BTB compartments, and correlated quantitatively with tumor burden in mice. The NIRF dyes and derivative dye-drug conjugates could be developed and further evaluated in men for cancer imaging and targeting.

Supplementary Material

Refer to Web version on PubMed Central for supplementary material.

Acknowledgments

This work was supported by NIH/NCI Grants 5P01CA098912, R01CA122602, the Board of Governors Cancer Research Chair, the Steven Spielberg Fund in Prostate Cancer Research, and a Margaret E. Early Medical Research Trust Award (to L.W.K.C.). We thank Mr. Gary Mawyer for editorial assistance.

References

1. Behin A, Hoang-Xuan K, Carpentier AF, Delattre JY. Primary brain tumours in adults. Lancet. 2003; 361:323–331. [PubMed: 12559880]
2. Wrensch M, Minn Y, Chew T, Bondy M, Berger MS. Epidemiology of primary brain tumors: current concepts and review of the literature. Neuro-oncology. 2002; 4:278–299. [PubMed: 12356358]
3. Kao HW, Chiang SW, Chung HW, Tsai FY, Chen CY. Advanced MR imaging of gliomas: an update. BioMed research international. 2013; 2013:970586. [PubMed: 23862163]
4. Wong TZ, van der Westhuizen GJ, Coleman RE. Positron emission tomography imaging of brain tumors. Neuroimaging clinics of North America. 2002; 12:615–626. [PubMed: 12687915]
5. de la Zerda A, Bodapati S, Teed R, Schipper ML, Keren S, Smith BR, et al. A comparison between time domain and spectral imaging systems for imaging quantum dots in small living animals. Molecular imaging and biology : MIB : the official publication of the Academy of Molecular Imaging. 2010; 12:500–508. [PubMed: 20012220]
6. Kantelhardt SR, Diddens H, Leppert J, Rohde V, Huttmann G, Giese A. Multiphoton excitation fluorescence microscopy of 5-aminolevulinic acid induced fluorescence in experimental gliomas. Lasers in surgery and medicine. 2008; 40:273–281. [PubMed: 18412229]
7. Agarwal S, Manchanda P, Vogelbaum MA, Ohlfest JR, Elmquist WF. Function of the blood-brain barrier and restriction of drug delivery to invasive glioma cells: findings in an orthotopic rat xenograft model of glioma. Drug metabolism and disposition: the biological fate of chemicals. 2013; 41:33–39. [PubMed: 23014761]
8. Groothuis DR. The blood-brain and blood-tumor barriers: a review of strategies for increasing drug delivery. Neuro-oncology. 2000; 2:45–59. [PubMed: 11302254]
9. Agarwal S, Sane R, Oberoi R, Ohlfest JR, Elmquist WF. Delivery of molecularly targeted therapy to malignant glioma, a disease of the whole brain. Expert reviews in molecular medicine. 2011; 13:e17. [PubMed: 21676290]

10. Lawson HC, Sampath P, Bohan E, Park MC, Hussain N, Olivi A, et al. Interstitial chemotherapy for malignant gliomas: the Johns Hopkins experience. Journal of neurooncology. 2007; 83:61–70.
11. Gu G, Gao X, Hu Q, Kang T, Liu Z, Jiang M, et al. The influence of the penetrating peptide iRGD on the effect of paclitaxel-loaded MT1-AF7p-conjugated nanoparticles on glioma cells. Biomaterials. 2013; 34:5138–5148. [PubMed: 23582684]
12. Zhang B, Sun X, Mei H, Wang Y, Liao Z, Chen J, et al. LDLR-mediated peptide-22-conjugated nanoparticles for dual-targeting therapy of brain glioma. Biomaterials. 2013; 34:9171–9182. [PubMed: 24008043]
13. Wu J, Pan D, Chung LW. Near-infrared fluoresence and nuclear imaging and targeting of prostate cancer. Transl Androl Urol. 2013; 2:254–264. [PubMed: 25285271]
14. Sevick-Muraca EM. Translation of near-infrared fluorescence imaging technologies: emerging clinical applications. Annual review of medicine. 2012; 63:217–231.
15. Yang X, Shi C, Tong R, Qian W, Zhau HE, Wang R, et al. Near IR heptamethine cyanine dye-mediated cancer imaging. Clinical cancer research : an official journal of the American Association for Cancer Research. 2010; 16:2833–2844. [PubMed: 20410058]
16. Yang X, Shao C, Wang R, Chu CY, Hu P, Master V, et al. Optical imaging of kidney cancer with novel near infrared heptamethine carbocyanine fluorescent dyes. The Journal of urology. 2013; 189:702–710. [PubMed: 23000848]
17. Shi C, Wu JB, Chu GC, Li Q, Wang R, Zhang C, et al. Heptamethine carbocyanine dye-mediated near-infrared imaging of canine and human cancers through the HIF-1alpha/OATPs signaling axis. Oncotarget. 2014; 5:10114–10126. [PubMed: 25361418]
18. Wu JB, Lin TP, Gallagher JD, Kushal S, Chung LW, Zhau HE, et al. Monoamine oxidase a inhibitor-near-infrared dye conjugate reduces prostate tumor growth. Journal of the American Chemical Society. 2015; 137:2366–2374. [PubMed: 25585152]
19. Wu JB, Shao C, Li X, Shi C, Li Q, Hu P, et al. Near-infrared fluorescence imaging of cancer mediated by tumor hypoxia and HIF1alpha/OATPs signaling axis. Biomaterials. 2014; 35:8175–8185. [PubMed: 24957295]
20. Xu Q, Yuan X, Tunici P, Liu G, Fan X, Xu M, et al. Isolation of tumour stem-like cells from benign tumours. British journal of cancer. 2009; 101:303–311. [PubMed: 19568241]
21. Xu J, Wang R, Xie ZH, Odero-Marah V, Pathak S, Multani A, et al. Prostate cancer metastasis: role of the host microenvironment in promoting epithelial to mesenchymal transition and increased bone and adrenal gland metastasis. The Prostate. 2006; 66:1664–1673. [PubMed: 16902972]
22. Wu JB, Shao C, Li X, Shi C, Li Q, Hu P, et al. Near-infrared fluoresence imaging of cancer mediated by tumor hypoxia and HIF1a/OATPs signaling axis. Biomaterials. 2014
23. Livak KJ, Schmittgen TD. Analysis of relative gene expression data using real-time quantitative PCR and the 2(-Delta Delta C(T)) Method. Methods. 2001; 25:402–408. [PubMed: 11846609]
24. Bredel M, Bredel C, Juric D, Harsh GR, Vogel H, Recht LD, et al. Functional network analysis reveals extended gliomagenesis pathway maps and three novel MYC-interacting genes in human gliomas. Cancer research. 2005; 65:8679–8689. [PubMed: 16204036]
25. Sun L, Hui AM, Su Q, Vortmeyer A, Kotliarov Y, Pastorino S, et al. Neuronal and glioma-derived stem cell factor induces angiogenesis within the brain. Cancer cell. 2006; 9:287–300. [PubMed: 16616334]
26. Vajkoczy P, Menger MD. Vascular microenvironment in gliomas. Cancer treatment and research. 2004; 117:249–262. [PubMed: 15015564]
27. Obaidat A, Roth M, Hagenbuch B. The expression and function of organic anion transporting polypeptides in normal tissues and in cancer. Annual review of pharmacology and toxicology. 2012; 52:135–151.
28. Bhowmik A, Khan R, Ghosh MK. Blood brain barrier: a challenge for effectual therapy of brain tumors. BioMed research international. 2015; 2015:320941. [PubMed: 25866775]
29. Roth M, Obaidat A, Hagenbuch B. OATPs, OATs and OCTs: the organic anion and cation transporters of the SLCO and SLC22A gene superfamilies. British journal of pharmacology. 2012; 165:1260–1287. [PubMed: 22013971]

30. Bronger H, Konig J, Kopplow K, Steiner HH, Ahmadi R, Herold-Mende C, et al. ABCC drug efflux pumps and organic anion uptake transporters in human gliomas and the blood-tumor barrier. Cancer research. 2005; 65:11419–11428. [PubMed: 16357150]

31. Ose A, Kusuhara H, Endo C, Tohyama K, Miyajima M, Kitamura S, et al. Functional characterization of mouse organic anion transporting peptide 1a4 in the uptake and efflux of drugs across the blood-brain barrier. Drug metabolism and disposition: the biological fate of chemicals. 2010; 38:168–176. [PubMed: 19833843]

32. Lu X, Kang Y. Hypoxia and hypoxia-inducible factors: master regulators of metastasis. Clinical cancer research : an official journal of the American Association for Cancer Research. 2010; 16:5928–5935. [PubMed: 20962028]

33. Wu JB, Shao C, Li X, Li Q, Hu P, Shi C, et al. Monoamine oxidase A mediates prostate tumorigenesis and cancer metastasis. J Clin Invest. 2014; 124:2891–2908. [PubMed: 24865426]

34. Tao XM, Wang JC, Wang JB, Feng Q, Gao SY, Zhang LR, et al. Enhanced anticancer activity of gemcitabine coupling with conjugated linoleic acid against human breast cancer in vitro and in vivo. European journal of pharmaceutics and biopharmaceutics : official journal of Arbeitsgemeinschaft fur Pharmazeutische Verfahrenstechnik eV. 2012; 82:401–409.

35. Daman Z, Ostad S, Amini M, Gilani K. Preparation, optimization and in vitro characterization of stearoyl-gemcitabine polymeric micelles: a comparison with its self-assembled nanoparticles. International journal of pharmaceutics. 2014; 468:142–151. [PubMed: 24731731]

36. Abratt RP, Bezwoda WR, Falkson G, Goedhals L, Hacking D, Rugg TA. Efficacy and safety profile of gemcitabine in non-small-cell lung cancer: a phase II study. Journal of clinical oncology : official journal of the American Society of Clinical Oncology. 1994; 12:1535–1540. [PubMed: 8040664]

37. Burris HA 3rd, Moore MJ, Andersen J, Green MR, Rothenberg ML, Modiano MR, et al. Improvements in survival and clinical benefit with gemcitabine as first-line therapy for patients with advanced pancreas cancer: a randomized trial. Journal of clinical oncology : official journal of the American Society of Clinical Oncology. 1997; 15:2403–2413. [PubMed: 9196156]

38. Carmichael J, Possinger K, Phillip P, Beykirch M, Kerr H, Walling J, et al. Advanced breast cancer: a phase II trial with gemcitabine. Journal of clinical oncology : official journal of the American Society of Clinical Oncology. 1995; 13:2731–2736. [PubMed: 7595731]

39. Hertel LW, Boder GB, Kroin JS, Rinzel SM, Poore GA, Todd GC, et al. Evaluation of the antitumor activity of gemcitabine (2',2'-difluoro-2'-deoxycytidine). Cancer research. 1990; 50:4417–4422. [PubMed: 2364394]

40. Ostruszka LJ, Shewach DS. The role of DNA synthesis inhibition in the cytotoxicity of 2',2'-difluoro-2'-deoxycytidine. Cancer chemotherapy and pharmacology. 2003; 52:325–332. [PubMed: 12811514]

41. Sigmond J, Honeywell RJ, Postma TJ, Dirven CM, de Lange SM, van der Born K, et al. Gemcitabine uptake in glioblastoma multiforme: potential as a radiosensitizer. Annals of oncology : official journal of the European Society for Medical Oncology / ESMO. 2009; 20:182–187. [PubMed: 18701427]

42. Evans TL, Kim JH, Shepherd FA, Syrigos KN, Udud K, Chubenko V, et al. Cabazitaxel (Cbz) versus topotecan in patients (pts) with small cell lung cancer (SCLC) that has progressed during or after first-line treatment with platinum-ased chemotherapy: A randomized phase II study. Journal of clinical oncology : official journal of the American Society of Clinical Oncology. 2013; 31

43. Preusser M, Berghoff AS, Schadendorf D, Lin NU, Stupp R. Brain metastasis: opportunity for drug development? Current opinion in neurology. 2012; 25:786–794. [PubMed: 23108247]

44. Seoane J, De Mattos-Arruda L. Brain metastasis: new opportunities to tackle therapeutic resistance. Molecular oncology. 2014; 8:1120–1131. [PubMed: 24953014]

45. Drake JM, Gabriel CL, Henry MD. Assessing tumor growth and distribution in a model of prostate cancer metastasis using bioluminescence imaging. Clinical & experimental metastasis. 2005; 22:674–684. [PubMed: 16703413]

46. Allard E, Passirani C, Benoit JP. Convection-enhanced delivery of nanocarriers for the treatment of brain tumors. Biomaterials. 2009; 30:2302–2318. [PubMed: 19168213]

47. Norden AD, Drappatz J, Wen PY. Antiangiogenic therapies for high-grade glioma. Nature reviews Neurology. 2009; 5:610–620. [PubMed: 19826401]

48. Kircher MF, de la Zerda A, Jokerst JV, Zavaleta CL, Kempen PJ, Mittra E, et al. A brain tumor molecular imaging strategy using a new triple-modality MRI-photoacoustic-Raman nanoparticle. Nature medicine. 2012; 18:829–834.

49. Hintersteiner M, Enz A, Frey P, Jaton AL, Kinzy W, Kneuer R, et al. In vivo detection of amyloid-beta deposits by near-infrared imaging using an oxazine-derivative probe. Nature biotechnology. 2005; 23:577–583.

50. Humblet V, Lapidus R, Williams LR, Tsukamoto T, Rojas C, Majer P, et al. Highaffinity near-infrared fluorescent small-molecule contrast agents for in vivo imaging of prostate-specific membrane antigen. Molecular imaging. 2005; 4:448–462. [PubMed: 16285907]

51. Wu X, Liu H, Liu J, Haley KN, Treadway JA, Larson JP, et al. Immunofluorescent labeling of cancer marker Her2 and other cellular targets with semiconductor quantum dots. Nature biotechnology. 2003; 21:41–46.

52. Jensen RL. Brain tumor hypoxia: tumorigenesis, angiogenesis, imaging, pseudoprogression, and as a therapeutic target. Journal of neuro-oncology. 2009; 92:317–335. [PubMed: 19357959]

53. Parney IF, Kunwar S, McDermott M, Berger M, Prados M, Cha S, et al. Neuroradiographic changes following convection-enhanced delivery of the recombinant cytotoxin interleukin 13-PE38QQR for recurrent malignant glioma. Journal of neurosurgery. 2005; 102:267–275. [PubMed: 15739554]

54. Harada H, Kizaka-Kondoh S, Itasaka S, Shibuya K, Morinibu A, Shinomiya K, et al. The combination of hypoxia-response enhancers and an oxygen-dependent proteolytic motif enables real-time imaging of absolute HIF-1 activity in tumor xenografts. Biochemical and biophysical research communications. 2007; 360:791–796. [PubMed: 17624305]

55. Buxhofer-Ausch V, Secky L, Wlcek K, Svoboda M, Kounnis V, Briasoulis E, et al. Tumor-specific expression of organic anion-transporting polypeptides: transporters as novel targets for cancer therapy. Journal of drug delivery. 2013; 2013:863539. [PubMed: 23431456]

56. Han S, Kim K, Thakkar N, Kim D, Lee W. Role of hypoxia inducible factor-1alpha in the regulation of the cancer-specific variant of organic anion transporting polypeptide 1B3 (OATP1B3), in colon and pancreatic cancer. Biochemical pharmacology. 2013; 86:816–823. [PubMed: 23924606]

57. Thompson BJ, Sanchez-Covarrubias L, Slosky LM, Zhang Y, Laracuente ML, Ronaldson PT. Hypoxia/reoxygenation stress signals an increase in organic anion transporting polypeptide 1a4 (Oatp1a4) at the blood-brain barrier: relevance to CNS drug 6 delivery. Journal of cerebral blood flow and metabolism : official journal of the International Society of Cerebral Blood Flow and Metabolism. 2014; 34:699–707.

58. Ihmels H, Thomas L. Light up G-quadruplex DNA with a [2.2.2]heptamethinecyanine dye. Organic & biomolecular chemistry. 2013; 11:480–487. [PubMed: 23203349]

59. Volkova KD, Kovalska VB, Balanda AO, Vermeij RJ, Subramaniam V, Slominskii YL, et al. Cyanine dye-protein interactions: looking for fluorescent probes for amyloid structures. Journal of biochemical and biophysical methods. 2007; 70:727–733. [PubMed: 17467807]

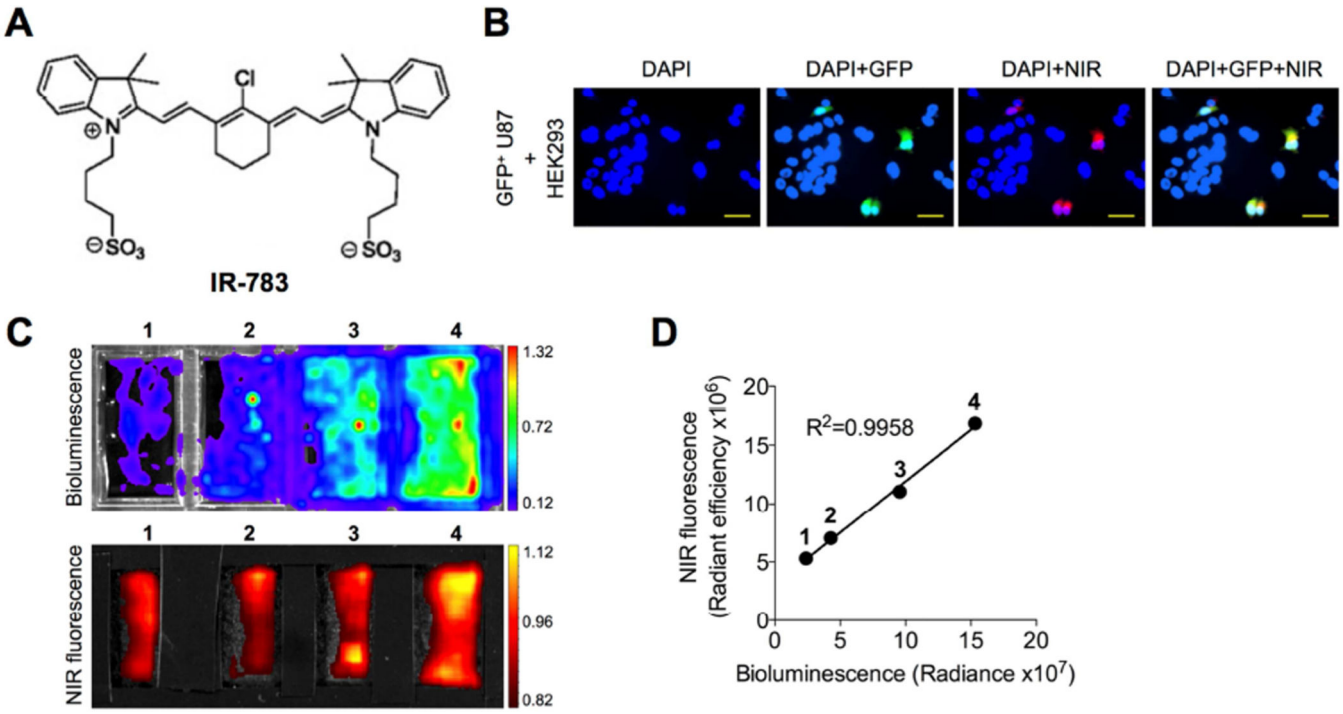

Fig. 1.

Uptake of NIRF heptamethine carbocyanine IR-783 dye by human glioblastoma cells. (A) Chemical structure of IR-783 dye. (B) Uptake of IR-783 dye (20 μM, 30 min) by GFP-tagged human glioblastoma U87 cells co-cultured with normal human HEK293 cells. Nuclei from both U87 and HEK293 cells were stained by DAPI. Scale bars represent 50 μm. (C) Uptake of luc-tagged U87 cells co-cultured with HEK293 cells at different ratios (U87/HEK293: 1, 1:8; 2, 1:4; 3, 1:2; and 4, 1:1) determined by both luminescence and NIRF imaging. (D) Correlation of luminescence and NIRF signal intensity in (C).

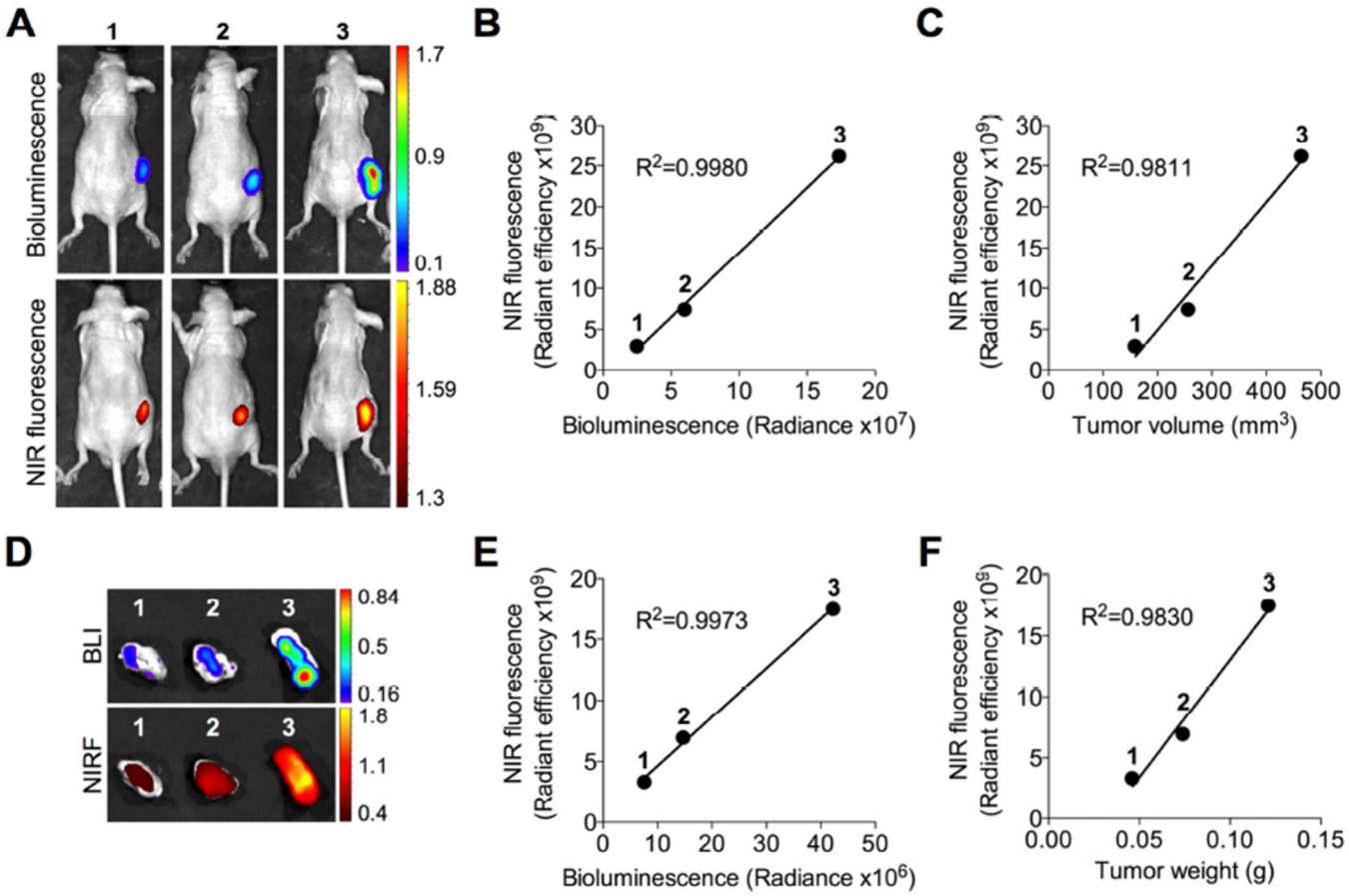

Fig. 2.

Preferential uptake and retention of IR-783 dye in subcutaneous U87 glioblastoma xenografts. (A) Uptake of IR-783 dye (50 nmol/mouse, i.p.) by subcutaneous luc-tagged U87 glioblastoma xenografts of different sizes determined by *in vivo* BLI and NIRF imaging (cell number initially implanted to form xenograft tumors: 1, 1×10^6; 2, 3×10^6; and 3, 9×10^6). (B, C) Correlation of tumor NIRF signal intensity with either BLI signal intensity (B) or tumor volume determined by caliper (C) in (A). (D) Uptake of IR-783 dye by U87 xenograft tumors dissected from (A) and determined by *ex vivo* BLI and NIRF imaging. (E, F) Correlation of tumor NIRF signal intensity with either BLI signal intensity (E) or tumor weight (F) in (d). n=3 for each experimental group. The mean was used to plot the correlation curves.

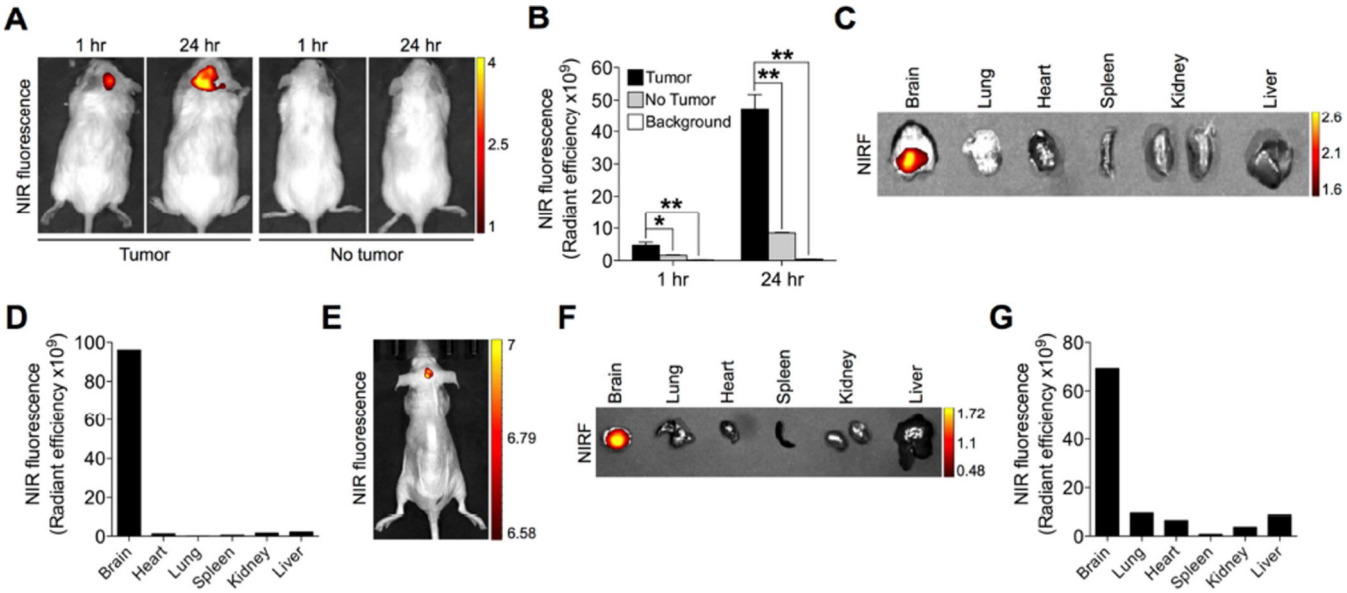

Fig. 3.

Preferential uptake and retention of IR-783 dye in intracranial brain tumor xenografts. (A) Uptake of IR-783 dye (50 nmol/mouse, i.p.) by intracranial U87 tumor 2 xenograft as determined by *in vivo* NIRF imaging at 1 hr and 24 hr time points after dye injection. Representative images are shown. (B) Quantitative analysis of uptake intensity in (A) (n=3, mean ± SEM). *$p<0.05$, **$p<0.01$. (C) Uptake and retention of IR-783 dye by representative mouse brain and other indicated organs dissected from (A), as determined by *ex vivo* NIRF imaging 24 hr after dye injection. (D) Quantitative analysis of NIRF signal intensity in (C). (E, F) Uptake of IR-783 dye (50 nmol/mouse, i.p.) by intracranial tumor developed originally from pituitary adenoma patient samples 24 hr after dye injection, which was further removed and subjected to *ex vivo* NIRF imaging in parallel with other organs (F). (G) Quantitative analysis of organ-specific NIRF signal intensity in (F).

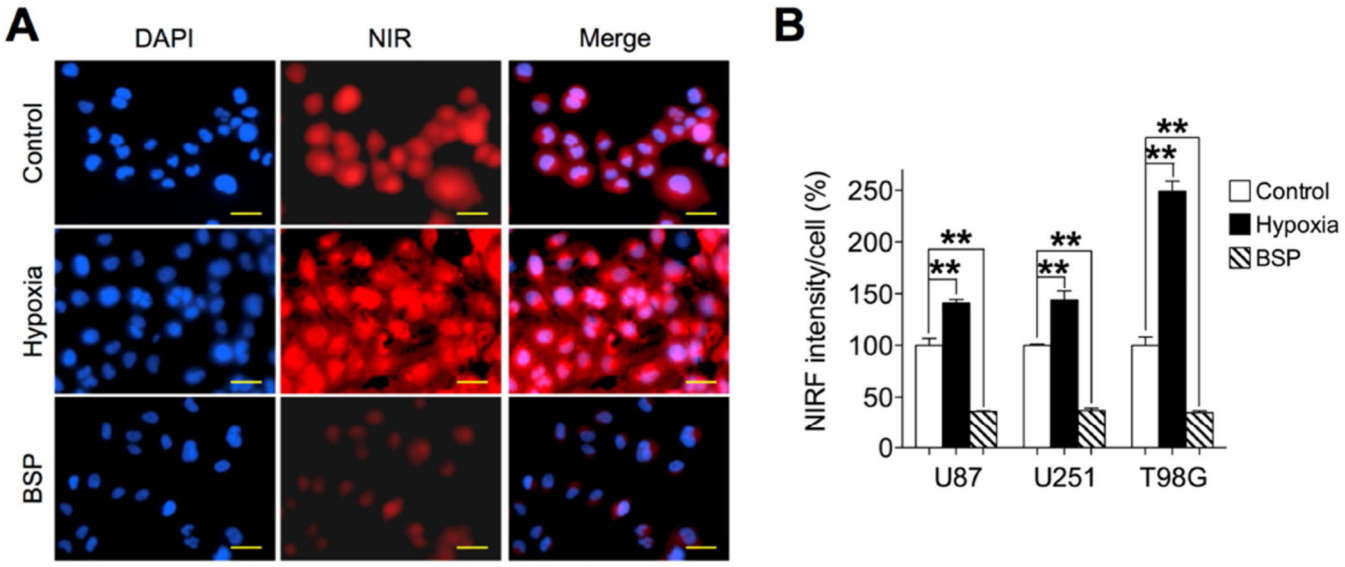

Fig. 4.

Hypoxia and OATP genes mediated the uptake of IR-783 dye by human glioblastoma cells. (A) Uptake of IR-783 dye (20 μM, 30 min) by U87 cells under pretreatment with either hypoxia (1% O_2, 1 hr) or bromsulphthalein (BSP) (250 μM, 1 hr). Scale bars represent 50 μm. (B) Quantitative analysis of NIRF signal intensity in U87, U251 and T98G cells. Intensity in control cells under normoxia and without treatment was set as 100% (n=5, mean ± SEM). ***p*<0.01.

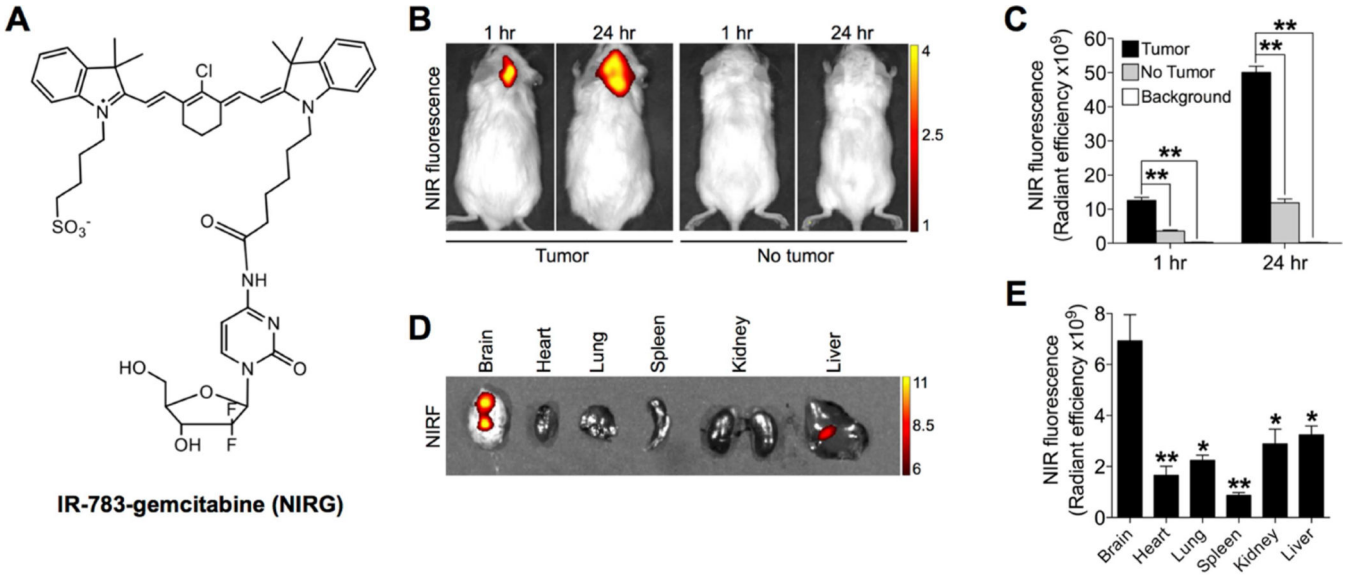

Fig. 5.

Uptake and retention of IR-783-gemcitabine dye-drug conjugate (NIRG) in intracranial U87 tumor xenografts. (A) Chemical structure of NIRG. (B) Uptake of NIRG (50 nmol/mouse, i.p.) by intracranial U87 tumor xenograft as determined by *in vivo* NIRF imaging at 1 hr and 24 hr time points after dye injection. Representative images are shown. (C) Quantitative analysis of uptake intensity in (A) (n=3, mean ± SEM). ***p*<0.01. 3 (D) Uptake and retention of NIRG by mouse brain and other indicated organs dissected from (B), as determined by *ex vivo* NIRF imaging 24 hr after dye injection. (E) Quantitative analysis of organ-specific NIRF signal intensity in (D). (n=3, mean ± SEM). **p*<0.05, ***p*<0.01 as compared to brain.

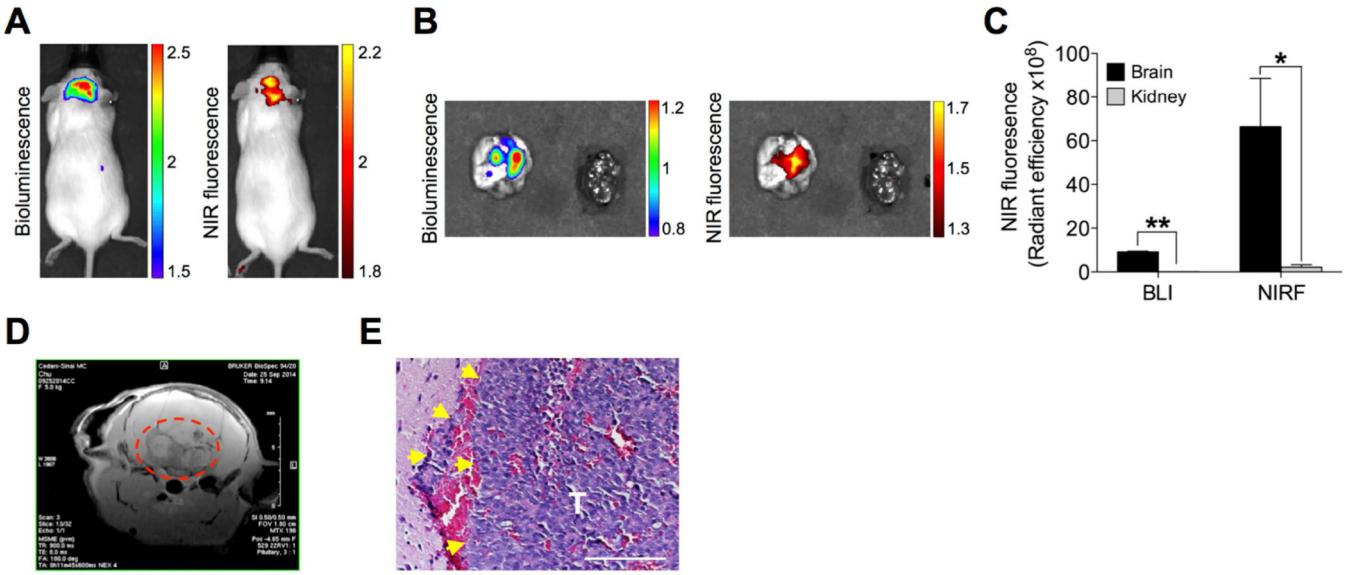

Fig. 6.

Uptake and retention of IR-783-gemcitabine dye-drug conjugate (NIRG) in xenograft prostate tumor brain metastases. (A, B) Mice bearing CW22Rv1 prostate tumor brain metastases were subjected to both BLI and NIRF imaging *in vivo* 24 hr after NIRG (50 nmol/mouse, i.p.) (A). Mouse brain and control kidney were subsequently excised and subjected *ex vivo* to both imaging modalities (B). (C) Quantitative analysis of both BLI and NIRF signal intensity in (B) (n=3, mean ± SEM). $^{**}p<0.05$, $^{**}p<0.01$. (D) MRI T2 scan of tumor-bearing mouse brain. Tumor area is indicated in red dashed circle. (E) H&E stain of prostate tumor brain metastases (T). Yellow arrows indicate invasive edges. Original magnification, ×400; scale bar: 20 μm.